# The Effects of Nonequilibrium Condensation on Shock/Boundary Layer Interaction

**Heuy-Dong Kim***
*Professor, Andong National University*
**Kwon-Hee Lee**
*BK21 Researcher, Andong National University*
**Toshiaki. Setoguchi**
*Professor, Saga University, Japan*

The effects of nonequilibrium condensation on the shock boundary layer interaction over a transonic bump model were investigated experimentally and numerically. An experiment was conducted using a supersonic indraft wind tunnel. A droplet growth equation was incorporated into two-dimensional Navier-Stokes equation systems. Computations were carried out using a third-order MUSCL type TVD finite-difference scheme with a second-order fractional time step. Computations compared with the experimental results. Nonequilibirum condensation suppressed the boundary layer separation and the pressure fluctuations due to the shock boundary layer interaction. Especially the nonequilibrium condensation was helpful to suppress the high frequency components of the pressure fluctuations.

**Key Words :** Compressible Flow, Nonequilibrium Condensation, Shock Wave, Transonic Flow, Shock Oscillation

## 1. Introduction

A rapid expansion of moist air or steam is presented in the flows through a transonic or supersonic nozzle and a turbine cascade and often gives rise to non-equilibrium condensation. The whole flow field is strongly affected by the latent heat released by the condensation of water vapor. The condensation phenomenon is essentially an irreversible process leading to appreciable entropy rise. If the heat release exceeds a certain critical value, it is known that nonequilibrium condensation leads to a discontinuous change of thermodynamic flow properties.(Wegener and Mach, 1958; Masuo et al., 1985; Zierep and Lin, 1967;Schnerr and Dehrmann, 1990)

The condensation shock wave has long been of scientific and academic research topic, and many thermodynamic and fluid dynamic aspects of nonequilibrium condensation and the condensation shock wave are well known now. The condensation shock wave almost always leads to large energy losses as well as flow instability due to the condensation shock wave oscillations, thereby affecting the whole system performance. (Barschdorff and Fillipov, 1990; Wegener and Cagliostro, 1973)

Many experimental and numerical investigations have been made to understand the relationship between the shock wave and nonequilibrium condensation.(Barschdorff and Eillipov, 1970; Wegener and Cagliostro, 1973; Saltanov Tkalenko, 1975; Matsuo et al., 1985) Much has been known about the effects of nonequilibrium condensation and the condensation shock wave on flow field. With nonequilibrium condensation upstream of the

* Corresponding Author,
**E-mail** : kimhd@andong.ac.kr
**TEL** : +82-54-820-5622; **FAX** : +82-54-841-1630
School of Mechanical Engineering, Andong National University, 388, Songchun-dong, Andong, Kyungpuk 750-749, Korea.(Manuscript **Received** October 9, 2000; **Revised** March 5, 2001)

shock wave, the flow Mach number decreases due to total pressure loss and latent heat released by the nonequilibrium condensation, consequently leading to suppression of shock-induced boundary layer separation. In addition, the fine droplets generated by the nonequilibrium condensation can alleviate the flow fluctuations downstream of the shock wave.

The nonequilibrium condensation leads to total pressure losses, which influence the interaction between shock wave and boundary layer. However the detailed effects of nonequilibrium condensation on the shock boundary layer interaction have not been fully understood yet. Moreover there are still many unknown problems for the effects of nonequilibrium condensation on the flow fluctuations occurring behind the shock wave.

The major objectives of the current study are to investigate the effects of nonequilibrium condensation on the shock wave boundary layer interaction which occurs in a transonic flow over a bump model. Nonequilibrium condensing flow was made by expansion of moist air over several bump models. An experiment was carried out to explore the effects of the initial conditions of the moist air flow and the bump configurations on the shock wave and flow fluctuations. Computations were made to predict the experimental results. Naveir-Stokes equations were solved numerically using a 3rd order MUSCL type TVD finite difference scheme with a 2nd order fractional step for time integration.

## 2. Experimental Facility and Procedure

A supersonic indraft wind tunnel is used to generate nonquilibirum condensation of atmospheric moist air in the test section. A vacuum chamber with a volume of $6m^3$ is connected to the test section, through which the controlled moist air in the upstream plenum chamber flows into the vacuum chamber. As schematically shown in Fig. 1, two bump models with a radius of 40mm and 200mm are installed on the lower wall of the test section. The chord lengths of the two bump

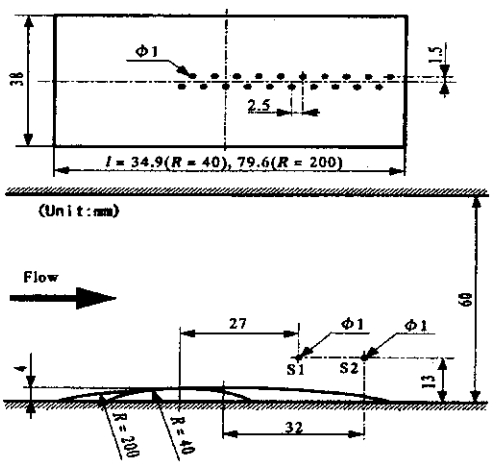


**Fig. 1** Schematic diagram of bump model

models are 34.9mm and 76.9mm, respectively, whill the height of the two models is fixed at 4. 0mm. Multiple pressure transducers are mounted flush on the bump models.

Time-mean and instantaneous pressures are measured using the pressure transducers. In addition, a schlieren optical system is used to observe the flow field over the bump models. In order to investigate the surface flow mehcanism over the bump models, shear sensitive liquid crystal (Merck Industrial Chemicals, TI622) is used for flow visualization.

A dryer system and a heater system controls the initial stagnation conditions of atmospheric air charged into the upstream plenum chamber. The stagnation temperature and relative humidity are measured by a thermometer and a humidity indicator. Steady flow over the bump models lasting for about 5 seconds is enough to implement the measurements required in the present work.

The stagnation pressure $P_{01}$ in the upstream plenum chamber is kept constant at 102kPa, and the stagnation temperature $T_{01}$ is set at 298K in the present experiment. The initial degree of supersaturation $S_{01}$, which defined as the ratio of the vapour pressure to the equilibrium saturation pressure corresponding to the plenum chamber temperature, is varied in the range from 0.24 to 0.80 where enable to occur nonequilibrium condensations in the transonic flows over bump

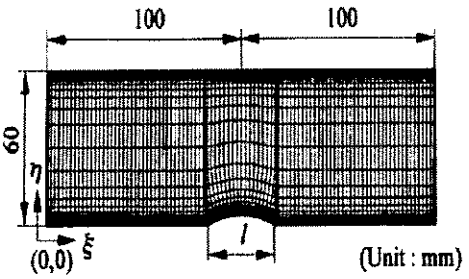


**Fig. 2** Computational grid

models. The static pressure P in the upstream of the bump model is measured. $P/P_{01}$ (=0.719) gives the flow Mach number of 0.735.

## 3. Navier-Stokes Computation

As in general two-phase flow analysis, several assumptions are made for the present computations. There is no velocity slip and no temperature difference between condensate particles and medium gas flows. Due to very small condensate particles, the effect of the particles on pressure field can be neglected.

The governing equations are unsteady two-dimensional, compressible, Navier-Stokes equations and a droplet growth equation(Sislian, 1975) written in the Cartesian coordinate system ($x$, $y$). The governing equations are non-dimensionalized using the reference values at the upstream plenum conditions and are in details given in Ref.(Kim and Setoguchi, 2000 (submitted); Setoguchi and Kim, 2000 (Submitted)).

Values of the accommodation coefficient (Wegener and Wu, 1977) for nucleation, condensation coefficient(Mills and Seban, 1967) and surface tension coefficient(Kirkwood and Buff, 1949) are 106, 0.9 and 1.29, respectively. Baldwin-Lomax model is used as a turbulence closure model in the present computations. The governing equation systems are mapped from the physical plane of the reference frame ($x$, $y$) into the computational plane ($\xi$, $\eta$) using general Coordinate transformations. A third order high resolution MUSCL type TVD finite difference scheme with a second order fractional step for time integration is applied to solve the governing equation systems and the droplet growth equation. A second order centered difference scheme is used for viscous terms. The detailed computational procedure is introduced in Ref. (Kim and Setoguchi, 2000(submitted); Setoguchi and Kim, 2000(Submitted))

Figure 2 shows the computational grid system. The grid contains 200 divisions in the $\xi$-direction and 60 divisions in the $\eta$-direction. The minimum dimensional length closest to the solid wall boundary is 0.0717mm. Free boundary conditions are applied to both inlet and exit boundaries. Adiabatic no-slip velocity is applied to the solid wall boundaries, in which condensate mass fraction g is assumed as g=0 on the wall. The conservative vector variables at the fictitious cells at both the inlet and exit boundaries are constrained with Riemann invariant. The value of the CFL number is fixed at 0.98 through out the whole computation.

## 4. Results and Discussion

### 4.1 Flow visualization

Figure 3 shows schlieren pictures for the transonic flows over R=40 and 200mm bump models. The initial degree of supersaturation $S_{01}$ was varied from 0.24 to 0.80. Note that for $S_{01}$= 0.24 the flow is assumed to be dry air in the present study. A weak normal transonic shock wave is clearly visible over the bump model. It is found that the shock structure is influenced by the bump model configuration significantly. The shock wave over the R=200mm bump extends nearly to the top wall, while that over the R= 40mm bump is limited to only the local area near the bump surface. With an increase in $S_{01}$, the shock wave becomes weaker and moves a little upstream. For $S_{01}$=0.80, no obvious shock wave is visible with only some weak wavelets. This results from the fact that the flow Mach number just upstream of the shock wave is reduced due to nonequilibrium condensation occurring over the bump model.

In order to investigate the flow phenomena at the foot of the shock wave over the bump, Fig. 4

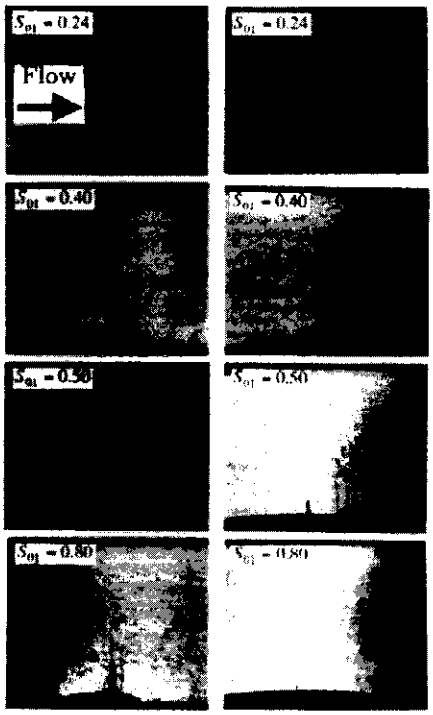


(a) $R$=40mm (b) $R$=200mm

**Fig. 3** Schlieren pictures

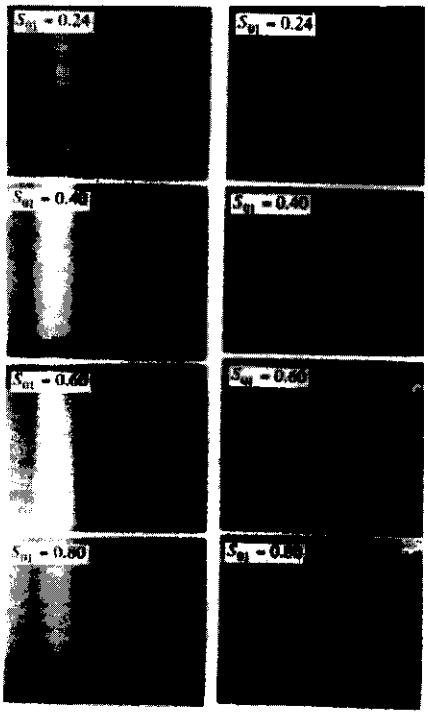


(a) $R$=40mm (b) $R$=200mm

**Fig. 4** Surface flow patterns

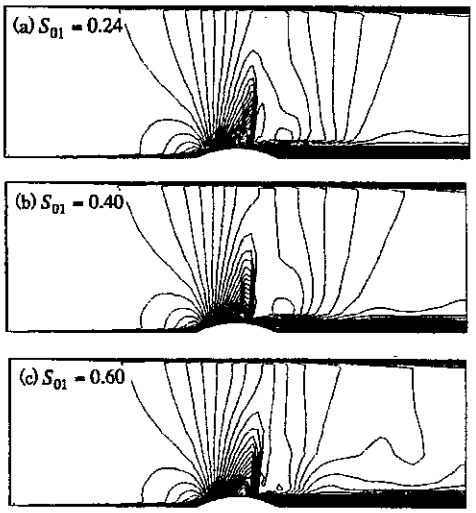


**Fig. 5** Computed Mach number contours(R = 40mm)

shows the surface flow patterns observed by liquid crystal. With the R=40mm bump model dry air flow separates just at the foot of the weak normal shock wave. This is due to the shock wave boundary layer interaction. With an increase in $S_{01}$ the flow does not separate at the foot of the shock wave, but separates just downstream of the shock wave. This boundary layer separation results from a sudden change of the flow area in the bump model and is different from the case of dry air flow, where the flow separates due to an adverse pressure gradient caused by the shock wave. It is noted that the boundary layer separation at the foot of the shock wave is suppressed as $S_{01}$ increases. However, with the R=200mm model the flow does not separate at the foot of the shock wave, nor any downstream location. The surface flow pattern does not change significantly with $S_{01}$.

A comparison of the present computations and experiments can be found in Fig. 5, in which Mach number contours are presented for the R= 40mm bump model. As observed in Fig. 3(a), the shock wave is nearly normal and limited to the local area over the bump model. It seems that the shock wave moves to upstream as $S_{01}$ increases, causing weaker shock wave. This trend is quite similar to the experimental results.

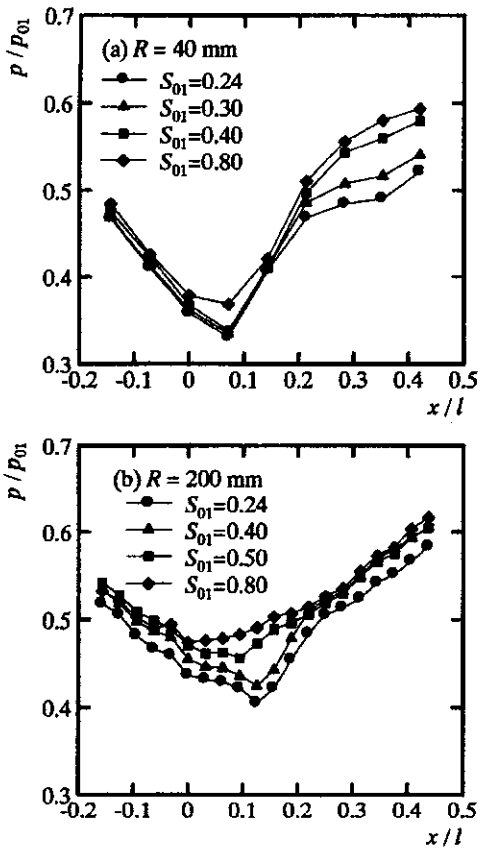


Fig. 6 Static wall pressures along bump model surface

### 4.2 Pressure measurement

Figure 6 shows the static wall pressures over the bump model. For both bump models the flow accelerates to the sonic speed at the bump apex and the flow becomes weakly supersonic downstream. This is terminated by the shock wave over the bump model. The static pressure decreases up to the location $x/l=0.07$ and then increases due to the shock wave. With an increase in $S_{01}$, the adverse pressure gradient of the shock wave seems to be reduced and the pressure recovery seems to be improved downstream. This results from nonequilibrium condensation which occurs upstream of the shock wave. It is reasonable to conclude that nonequilibrium condensation suppresses the flow separation due to the shock boundary layer interaction.

Figure 7 shows comparison of the present

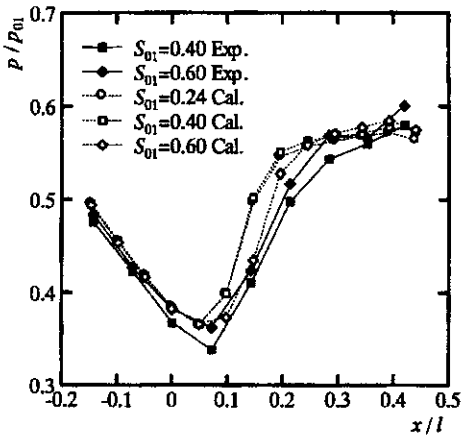


Fig. 7 Computed and measured static wall pressures

computations and experimental results. Similar trends are observed in both results, although the present computations seem to overpredict the static pressures over the bump model. However the present computational results may be accepted as reasonable in that the bump model contains very complicated flow phenomena like shock boundary layer interaction and nonequilibrium.

### 4.3 Effect of nonequilibrium condensation on pressure fluctuations

Figure 8 shows the experimental results of the fluctuating wall pressures over the bump models.

Root mean square values $P_{rms}$ of the fluctuating wall pressures are normalized by local mean pressure values. For R=40mm and $S_{01}$= 0.24, the peak value of fluctuating wall pressure is about 3.3% of local mean pressure value and seems to occur at the foot of the shock wave. With an increase in $S_{01}$, the peak values seem to reduce and move to a little upstream. With regard to the effect of R on the fluctuating wall pressures, it seems that the peak values of fluctuating wall pressure decreases as R increases. For the same $S_{01}$ of 0.80, the peak value over the R=200mm bump model is much lower than that over R= 40mm model. From the present experimental results, it is concluded that nonequilibrium condensation reduces the pressure fluctuations due to the shock boundary layer interaction. The interaction of the shock wave with the

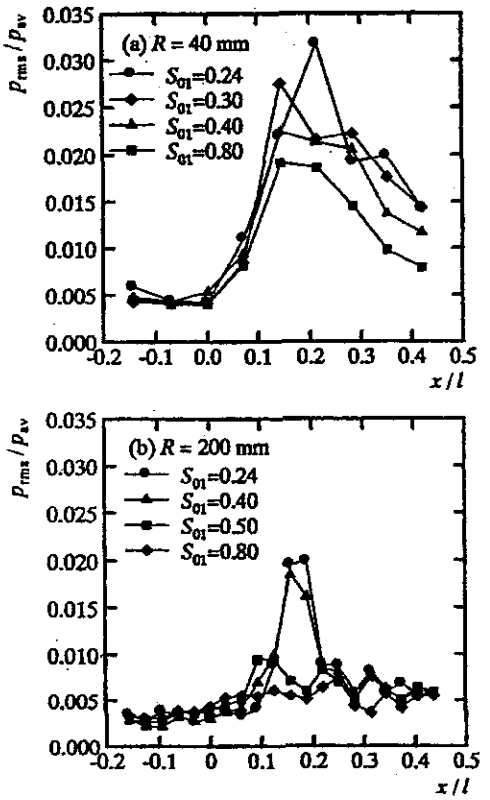


**Fig. 8** Root-mean-square values of pressure fluctuations

boundary layer becomes weak with an increase in $S_{01}$.

The fine droplets of nonequilibrium Condensation can influence the interaction as well. Detailed mechanism of the effects of the fine droplets on shock boundary layer interaction should be known to address this difficult problem.

Further information on the time scale of the fluctuating pressure signals can be obtained from the wavelet transform(Farge, 1992), as has frequently been applied to time-dependent data analysis. Using the fluctuating pressure signals, the present study has conducted the analysis of a continuous wavelet transform W($b$, $a$) as described next.

For the time-dependent pressure signals p($t$), the continuous wavelet transform W is defined by,

$$W(b,\ a)=\frac{1}{a^{1/2}}\int_{-\infty}^{\infty}\psi\left(\frac{t-b}{a}\right)p(t)dt \qquad (1)$$

Where $\psi$ is a mother wavelet, a the scale parameter and b the location of time scale. Therefore the wavelet tranform $W(b,\ a)$ provides us multi-scale structures of the pressure signals on the ($b$, $a$) frame. The mother wavelet, called Morley wavelet(Farge, 1992), is given as,

$$W(t)=(b,\ a)=\exp(i\kappa_\phi T)\exp\left(-\frac{T^2}{2}\right) \qquad (2)$$

$$T=\frac{t-b}{a} \qquad (3)$$

where $\kappa_\phi$ is a constant($\kappa_\phi$=6.0). The real part of the Morley wavelet above is symmetric with respect to T=0. The value of 1/a is taken to be the same as the frequency.

Figures 9 and 10 show the experimental results obtained from the present wavelet transform analysis. The wavelet coefficient $W(b,\ a)$ was plotted using the fluctuating pressure signals at measuring points S1 and S2, as shown in Fig. 1. Each contour line means the line of $W$=0. From both the figures, it is found that the dense region of the contours lines appears to be at equal intervals on the b-axis, being containing the range from high to low frequency. The dense region of high frequency results from boundary layer separation. For $S_{01}$=0.80, the contour lines in the region of high frequency become sparse rather, but in the low frequency region the contour lines are not significantly different from those of $S_{01}$=0.24. This means that nonequilibrium condensation suppresses the high frequency components of the fluctuating pressure signals, which are caused by the shock boundary layer interaction

From the results in Fig. 9 and 10, it is also found that the bump geometry can influence the whole components of the fluctuating pressure signals.

### 4.4 Total pressure loss

Due to nonequilibrium condensation and the shock wave, total pressure losses are expressed by entropy change(Sugawara and Oshima, 1968) as,

$$s-s_{01}=(1-\omega_{01})\frac{\Re}{Ma}\ln\left(T^{(\gamma_a/(\gamma_a-1))}\right)$$

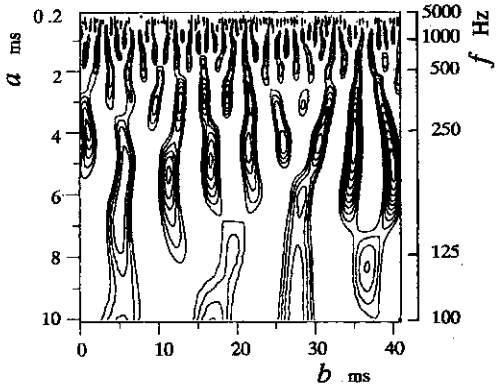


(a) $S_{01}=0.24$

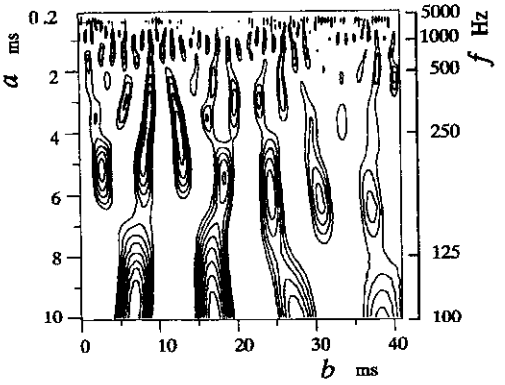


(b) $S_{01}=0.80$

**Fig. 9** Wavelet transform of time-dependent pressure signals(R=40mm)

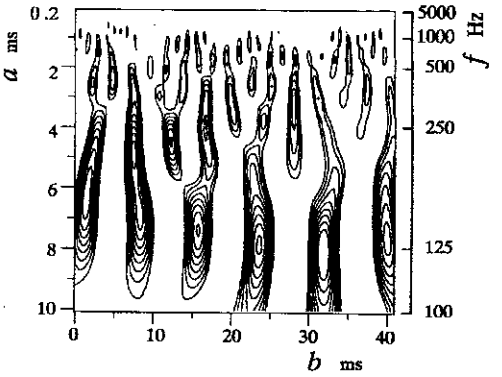


(a) $S_{01}=0.24$

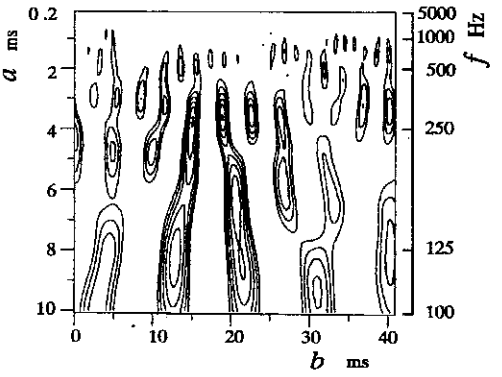


(b) $S_{01}=0.80$

**Fig. 10** Wavelet transform of time-dependent pressure signals(R=200 mm)

$$+(\omega_{01}-g)\frac{\Re}{M_v}\ln(T^{(\gamma_a/(\gamma_a-1))}/P_v)$$

$$+g\left(-\frac{1}{\gamma}\frac{3}{\rho_t}\frac{\partial\sigma}{\partial T}\right) \quad (4)$$

$$\frac{s-s_{01}}{c_p}=\ln\left(\frac{T_0}{T_{01}}\right)-\frac{\Re}{M_m c_p}\ln\left(\frac{p_0}{p_{01}}\right) \quad (5)$$

Figure 11 show the contour lines of the total pressure $(P_{01}-P_0)/P_{01}$, where $P_{01}$ means the total pressure upstream of the bump model and $P_0$ the local total pressure.

The total pressure loss seems to be concentrated at the regions, where the shock wave, shear layer, and boundary layer occur. The region of the major total pressure loss expands with an increase in $S_{01}$. Increase in $S_{01}$ consequently tends to reduce the strength of the shock wave and to suppress the boundary layer separation. In this study , it is not easy to discuss each of the major causes contributing to the total pressure loss. However

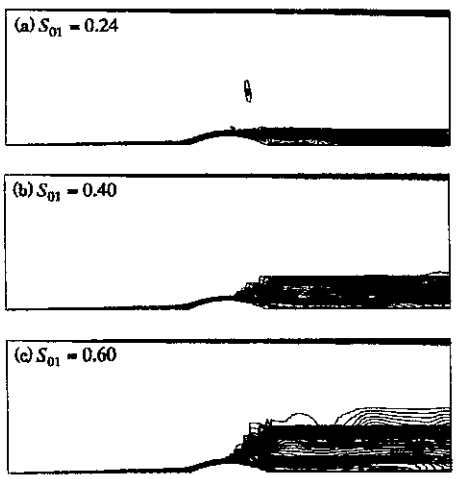


**Fig. 11** Total pressure loss contours (R=40mm)

the total pressure loss due to nonequilibrium condensation should be considered from the point of view of the entire energy loss.

## 5. Concluding Remarks

Experiments were conducted using a supersonic indraft wind tunnel. In order to investigate the effects of nonequilibrium condensation on the shock boundary layer interaction over a bump model. Two-dimensional compressible Navier-Stokes equations were solved using the TVD MUSCL finite difference scheme. Non-equilibirum condensation suppressed the separation and the pressure fluctuations caused by shock boundary layer interaction. Especially nonequilibrium condensation was helpful to suppress the high frequency components of the pressure fluctuations. Further study is required to address the detailed flow mechanisms for the fine droplet effects on the shock boundary layer interaction.

## Acknowledgements

This work was supported by the Brain Korea 21 project in 2001.

## References

Barschdorff, D. and Fillipov, G. A., 1970, "Analysis of Certain Special Operating Modes of Laval Nozzles with Local Heat Supply," *Heat Transfer-Society Research*, Vol. 2, No. 5, p. 76 ~87.

Farge, M., 1992, "Wavelet Transforms, Their Applications to Turbulence," *Annual Review of Fluid Mechanics*, Vol. 24, pp. 395~457.

Kim, H.D. and Setoguchi, T., 2000, "Passive Condensation Shock Wave in a Transonic Flows," *Intl. Jour. Heat and Mass Transfer* ( submitted)

Kirkwood, J. G. and Buff, F. P., 1949, "The Statistical Mechanical Theory of Surface Tension," *J. Chem. Phys.*, Vol. 17, pp. 3389~3343.

Matsuo, K. and Kawagoe, S. and Sonoda, K. and Sakao, K., 1985, "Studies of Condensation Shock Waves(Part I, Mechanism of their Formation)," *Bulletin of JSME*, Vol. 28, No. 241, pp1416~1422.

Matsuo, K. and Kawagoe, S. and Sonoda, K. and Setoguchi, T., 1985, "Oscillations of Laval Nozzle Flow with Condensation (Part 2, On the Mechanism of Oscillations and Their Amplitudes)," *Bulletin of JSME*, Vol. 28, No. 235, pp. 88~93.

Mills, A. F. and Seban, R. A., 1967, "The Condensation Coefficient of Water," *Int. J. Heat Mass Transf.*, Vol. 10, pp. 1815~1827.

Saltanov, G. A. and Tkalenko, R. A., 1975, "Investigation of Transonic Unsteady State Flow in the Presence of Phase Transformations," *J. of Appl. Mech. Tech. Phys.*, Vol. 16, No. 6, pp. 857 ~878.

Schnerr, G.H. and Dohrmann, U., 1990, "Transonic Flow Around Airfoils with Relaxation and Energy Supply by Homogeneous Condensation," *AIAA Journal.*, Vol. 28, No. 7, pp. 1187~1193.

Setoguchi, T. and Kim. H. D., 2000, "*Passive Control of Condensation Shock Oscillations in a Transonic Nozzle*," Intl. Jour. Heat and Mass Transfer(submitted)

Sislian, J.P., 1975, "Condensation of Water Vapour with or without a Carrier Gas in s Shock Tube," *UTIAS Rep. 201.*

Sugawara, M. and Oshima, N., 1968, "Analysis of Condensation in Supersonic Nozzles," *Proc. 12th Intl. Symp. on Combustion*, pp. 1193~1201.

Wegener, P. P. and Mach, L. M., 1958, "Condensation in Supersonic Hypersonic Wind Tunnels," *Adv. In Appl Mech.*, Vol. 5 pp. 307 ~447 Academic Press.

Wegener, P.P. and Cagliostro, D. J., 1973, "Periodic Nozzle Flow with Heat Addition," *Combustion Science and Technology*, Vol. 6, pp. 269~277.

Wegener, P.P., Wu, B., 1977, "Nucleation Phenomena," pp. 325.

Zierep, J. and Lin, S., 1967, "Bestimmung des Kondensationsbeginns Kondensation Bei Entspannung feuchter Luft in Ueberschallduesen," *Forsch. Ing. Wes.*, Vol. 33, pp. 169 ~172.